The FASEB Journal article fj.08-125286. Published online January 6, 2009.

Crystal structure of human esterase D: a potential genetic marker of retinoblastoma

Dong Wu, Yang Li, Gaojie Song, David Zhang, Neil Shaw,[1] and Zhi-Jie Liu[1]

National Laboratory of Biomacromolecules, Institute of Biophysics, Chinese Academy of Sciences, Beijing, China

ABSTRACT **Retinoblastoma (RB), a carcinoma of the retina, is caused by mutations in the long arm of chromosome 13, band 13q14. The *esterase D* (*ESD*) gene maps at a similar location as the *RB* gene locus and therefore serves as a potential marker for the prognosis of retinoblastoma. Because very little is known about the structure and function of ESD, we determined the 3-dimensional structure of the enzyme at 1.5 Å resolution using X-ray crystallography. ESD shows a single domain with an α/β-hydrolase fold. A number of insertions are observed in the canonical α/β-hydrolase fold. The active site is located in a positively charged, shallow cleft on the surface lined by a number of aromatic residues. Superimposition studies helped identify the typical catalytic triad residues—Ser-153, His264, and Asp230—involved in catalysis. Mutagenesis of any of the catalytic triad residues to alanine abolished the enzyme activity. Backbone amides of Leu54 and Met150 are involved in the formation of the oxyanion hole. Interestingly, a M150A mutation increased the enzyme activity by 62%. The structure of human ESD determined in this study will aid the elucidation of the physiological role of the enzyme in the human body and will assist in the early diagnosis of retinoblastoma. Wu, D., Li, Y., Song, G., Zhang, D., Shaw, N., Liu, Z. J. Crystal structure of human esterase D: a potential genetic marker of retinoblastoma. *FASEB J.* 23, 000–000 (2009)**

Key Words: Wilson disease · X-ray · endogenous uveitis · hydrolase fold · carcinoma

The esterase d (*ESD*) gene has been studied extensively due to its close proximity to the gene responsible for retinoblastoma (1, 2). Retinoblastoma (RB), a cancer of the eye, generally affects children and, if diagnosed early, is curable. Unattended RB cases, especially seen in developing countries, result in complications and death (3). Correct early diagnosis is even more so important, because the onset of the disease is very similar to another abnormality affecting the retina, Coats' disease. Often Coats' disease symptoms are misdiagnosed as retinoblastomas, resulting in unnecessary enucleations being performed on patients (4). Because *ESD* gene maps close to the *RB* gene locus on the long arm of chromosome 13, band 13q14, it has been often used successfully as a genetic marker for diagnosis of RB cases. *ESD* has also been successfully employed as a prognostic tool in many cases to assess an individual's genetic predisposition to RB (5, 6). Screening of ESD activity in all patients of RB has been emphasized in order to account for fairly small chromosome deletions that could potentially escape detection (7). In addition to RB diagnosis, *ESD* has found application as a genetic marker for Wilson's disease. Wilson's disease is caused by mutations in the *ATP7B* gene, resulting in accumulation of toxic levels of copper in tissues. The *ATP7B* gene maps to the same subband of chromosome 13, 13q14, as the *ESD* gene. Because *ESD* and *ATP7B* genes are tightly linked, *ESD* could potentially aid the diagnosis of Wilson's disease (8–11).

In a recent study, autoantibodies were detected against ESD in mice with experimental autoimmune uveoretinitis (EAU) (12). On the basis of these findings, when patients with Behcet's disease (BD) and Vogt-Koyanagi-Harada disease (VKH) were tested for the presence of autoantibodies against ESD, 25% tested positive. BD and VHK are sight-threatening ocular inflammations. Although the pathogenesis of these diseases is not clear, the symptoms have been linked to the development of autoimmunity against certain antigens, such as ESD, β-actin, tubulin β-2, creatine kinase, voltage-dependent anion-selective channel protein, and aspartate aminotransferase (12).

In spite of its medical significance, very little is known about the structure and function of the ESD protein (13). Varki *et al.* (14) have previously shown that ESD extracted from human erythrocytes could specifically cleave the *O*-acetyl ester linkage at the exocyclic C9 position of 9-*O*-acetyl-*N*-acetylneuraminic acid. Such highly specific 9-*O*-acetyl esterase activity is employed by influenza C virus and bovine coronavirus to destroy the receptors and release the progeny. Destruction of the receptor prevents aggregation of the progeny and nonproductive binding. The 9-*O*-acetyl esterase activity of human ESD has been postulated to play a role in recycling of the sialic acid. Interestingly, treatment of a promonocytic cell line with phenobarbital resulted in a 3-fold increase in the levels of expression of ESD, indicating a role for ESD in detoxification (15). However, the precise biological function and physiological role of ESD still remain unclear. Biochemi-

[1] Correspondence: National Laboratory of Biomacromolecules, Institute of Biophysics, 15 Datun Lu, Beijing 100101, China. E-mail: N.S., neilshaw@moon.ibp.ac.cn; Z.J.L., zjliu@ibp.ac.cn

doi: 10.1096/fj.08-125286

cal studies carried out on ESD indicate that *p*-chloromercuribenzoate, diisopropyl fluorophosphonate (DFP), phenylmethylsulfonyl fluoride, fluoride, and mercuric chloride inhibit the enzyme activity significantly (16, 17).

We decided to determine the 3-dimensional (3D) structure of human esterase D (also known as S-formylglutathione hydrolase) in an attempt to obtain clues about its function and possible physiological role.

MATERIALS AND METHODS

Protein production

ESD gene was amplified from human brain cDNA library using the following primers: forward 5′-TACTTCCAATCCAATGCTATGGCATTGAAGCAG-3′, reverse 5′-TTATCCACTTCCAATGTCATGCATTCAGGTATT-3′. The PCR product was ligated into pMCSG7 vector (18). The protein was expressed with an *N*-terminal hexahistine tag in *Escherichia coli* BL21 (DE3) cells. Cells were grown in Luria Bertani Medium at 37°C until the OD_{660nm} reached 0.8. Recombinant protein production was initiated by first cooling the culture to 16°C, followed by addition of 0.2 mM isopropyl-β-D-thiogalactoside (IPTG). After 20 h, the cells were harvested by centrifugation, sonicated, clarified, and loaded on an Ni-affinity column. After rigorous washing with PBS (50 mM Na_2HPO_4, 10 mM KH_2PO_4, 137 mM NaCl, 2.7 mM KCl, pH 7.4) containing 20 mM imidazole, the bound protein was eluted with an elution buffer containing 300 mM imidazole. Imidazole was removed by buffer exchange, and the His tag was cleaved by treating the protein with tabacco etch virus (TEV) protease. Uncut protein and TEV was removed by using a second Ni-affinity chromatography step. The protein was concentrated and loaded on a Superdex G75 size exclusion column equilibrated with 20 mM Tris-HCl, pH 8.0; 200 mM NaCl; and 1 mM dithiothreitol. Fractions containing the protein were pooled, concentrated to 10–15 mg/ml, and immediately screened for crystallization.

Esterase assay

The ESD activity was measured by a Hitachi F-4500 fluorometer (Hitachi, Tokyo, Japan) using 4-methylumbelliferyl acetate as a substrate. ESD was incubated with 5 mM substrate in 400 μl of 50 mM KH_2PO_4/Na_2HPO_4 and 150 mM NaCl, pH 7.4, at 25°C for 2 min. The reaction was stopped by the addition of 600 μl of 50 mM citric acid. The cleaved methylumbelliferone was excited at 360 nm and quantitated by measuring its emission at 460 nm. One unit of enzyme activity was defined as the amount of 4-methylumbelliferone released per minute under the assay conditions. All assays were performed in triplicate under identical conditions with appropriate controls. The protein concentration was estimated by reading the absorbance at 280 nm. An extinction coefficient of 50,350 M^{-1} cm^{-1} was used to calculate the amount of protein in milligrams per milliliter.

Site-directed mutagenesis

Mutagenesis was carried out using QuikChange site-directed mutagenesis kit (Stratagene, La Jolla, CA, USA) following the manufacturer's instructions. Mutants were expressed, purified, and assayed under identical conditions as the wild-type ESD.

Crystallization

Crystallization screening was done at 16°C using commercially available sparse matrix screens. Drops were set up using Mosquito (TTP Lab Tech, Royston, UK) crystallization robot. Hanging drops (0.6 μl) containing equal amounts of protein and mother liquor were equilibrated against 50 μl reservoir solution. Crystals appeared within 3 days in a solution containing 100 mM sodium citrate, pH 5.6; 200 mM ammonium acetate; and 30% (w/v) PEG 4000. The crystals belonged to space group $P2_1$ with unit cell dimensions a = 51.54 Å, b = 70.72 Å, c = 65.01 Å; α = 90.00°, β = 108.84°, γ = 90.00°.

Structure determination

Crystals were frozen in liquid nitrogen prior to diffraction testing and data collection. Native diffraction data were collected at a wavelength of 0.979 Å at beamline 19-ID, Advanced Photon Source (Argonne National Laboratory, Lemont, IL, USA). Data were indexed and scaled to 1.5-Å resolution using HKL2000 (19). The structure was solved by molecular replacement using Molrep with structure of a hypothetical protein from yeast (PDB code 1PV1) as a search template (20). The asymmetric unit consists of 2 molecules of ESD based on the calculated Matthews coefficient value of 1.81 $Å^3$/Da and a solvent content of 32.17%. Electron density for most of the peptide backbone was of good quality, except for residues Lys91 to Asp98, Gly213 to Gln215, Thr194, and Asp195 from chain A; Met1, Ala2, and Glu41 to Lys44 from chain B could not be traced. Refinement was carried out using REFMAC (21). Five percent of the unique reflections was assigned, in a random fashion, to the "free" set, for calculation of the free R factor (R_{free}), the remaining 95% of the reflections constituted the "working" set, for calculation of R (22). Manual adjustments to the model were done using COOT (23). Details of data collection and refinement statistics are listed in **Table 1**. The quality of the final model was validated with MOLPROBITY (24).

TABLE 1. *Data collection and refinement statistics*

Statistic	Native
Data collection	
Space group	$P2_1$
Cell dimensions	
a, *b*, *c* (Å)	51.54, 70.72, 65.01
α, β, γ (deg)	90.00, 108.84, 90.00
Resolution (Å)[a]	50.0–1.5 (1.53–1.50)
R_{sym}	0.073 (0.325)
$I/\sigma(I)$	20.47 (2.30)
Completeness (%)	98.4 (99.3)
Redundancy	3.6 (3.5)
Refinement	
Resolution (Å)	40.16–1.50
Reflections	65,767
R_{work}/R_{free}	0.1758/0.1961
Atoms	
Protein	4257
Water	616
B factors	
Protein	15.83
Water	32.61
RMS deviations	
Bond lengths (Å)	0.006
Bond angles (deg)	1.034
Geometry	
Most favored regions (%)	97.4
Allowed regions (%)	2.6
All atom clash score	5.5

[a]Highest-resolution shell is shown in parenthesis.

RESULTS

Overall structure

The secondary structural elements of ESD are arranged in a typical α/β-hydrolase fold (**Fig. 1**). A central sheet made up of 9 β strands arranged in a highly twisted superhelical structure is surrounded by α helices on either side. While strands β1 and β3 run antiparallel, the remaining strands of the sheet are parallel. ESD has 10 helices, with α1, α2, and α10 packed against the concave side of the central twisted sheet. Two of these helices (α5 and α8) are insertions in the canonical fold. A long loop (Pro85-Met124) is inserted between strand β5 and helix α3. Similar caplike insertions in the canonical α/β-hydrolase fold have been reported before and are postulated to confer substrate specificity and in some cases exclude reactants from the solvent. Primary sequence analysis revealed the presence of GxSxG motif, commonly observed in esterases. The characteristic catalytic triad residues of the α/β-hydrolase fold—Ser-149, Asp226, and His260—could be identified and are located inside the putative active site cleft (**Fig. 2**). The catalytic Ser-149 displays strained geometry (backbone angles φ=62.6, ψ=−115) in order to place the adjoining Met150 backbone amide nitrogen in the oxyanion hole. This is consistent with its highly conserved role of nucleophilic elbow, a hallmark of all α/β-hydrolases. In addition to Met150, the backbone amide of Leu54 participates in the formation of oxyanion hole.

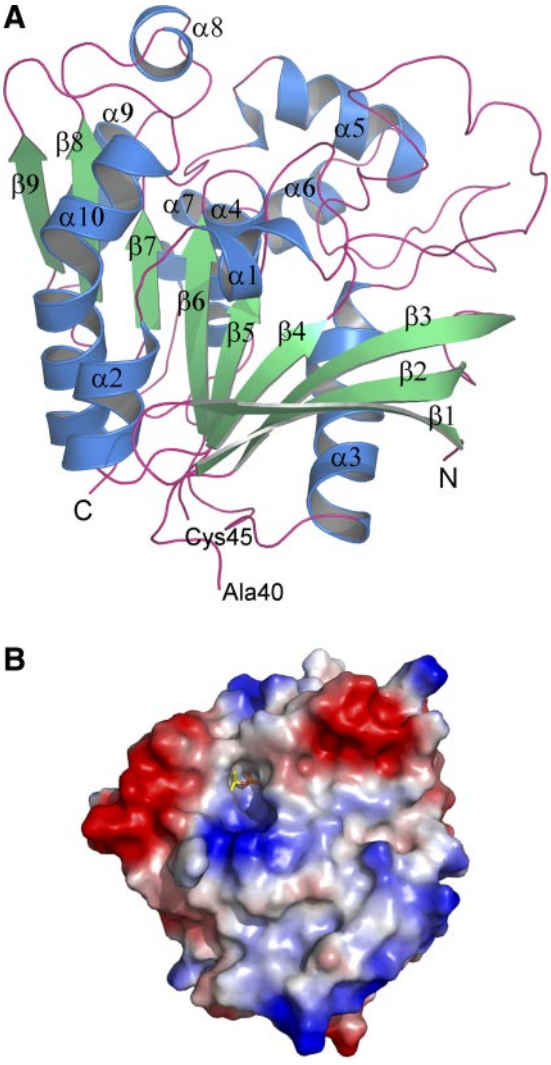

Figure 1. Overall structure of human ESD. *A*) Cartoon representation of the structure. N and C terminals of the protein are marked. Density for residues 41–44 was missing. *B*) Surface representation showing the distribution of electrostatic potential. The superimposed DFP ligand (shown as sticks) sits in a positively charged cavity. Blue, positive potential; red, negative potential.

Active site

Because cocrystallization and soaking experiments failed to yield intepretable density for the 4-methylumbelliferone acetate substrate, insights into the active site of ESD could be gained by superimposing the DFP inhibitor of IroE (PDB code 2GZS) over the structure of ESD (25). The inhibitor superimposes within the putative active site cleft of ESD and is in close proximity of the catalytic nucleophile Ser-149 (Figs. 1*B* and 2). The side chain of Ser-149 overlaps well with the equivalent catalytic Ser-189 of IroE. The distance between the Oγ oxygen of Ser-149 and modeled position of the phosphate atom of the superimposed DFP is 2.6 Å. This arrangement could be interpreted as Ser-149 of ESD, forming an adduct with DFP similar to that seen in IroE. The catalytic His260 (equivalent to His287 in IroE) is within hydrogen bonding distance of the Ser-149. The carboxyl oxygen of the catalytic acid, Asp226, is seen forming a 2.5 Å hydrogen bond with the N1 nitrogen of the His260 (Fig. 2*B*). An equivalent catalytic acid could not be identified in IroE, since this region is disordered in the structure of IroE. In this model, the amide nitrogens of Met150 and Leu54 could form a hydrogen bond with the free O3 oxygen of the DFP inhibitor. Interestingly, IroE employs the backbone amide of Tyr190 and the NH1 and NH_2 atoms of Arg130 in the oxyanion hole. Unlike IroE, the active site of ESD is lined with a number of aromatic residues like His148, Phe172, Trp183, Phe228, His260, and Tyr262. These features are reminiscent of carbohydrate binding sites and are primarily used for docking substrates containing aromatic rings. The physiological substrate of ESD is therefore likely to contain an aromatic moiety. ESD could cleave 4-methylumbelliferone acetate efficiently when assayed under standard conditions (**Table 2**). ESD has also been shown to remove acetyl groups from the C9 position of *O*-acetylated sialic acid derivatives (14). Both of these substrates contain aromatic moieties.

The mechanism of hydrolysis of the substrate is highly conserved in esterases and proceeds *via* the formation of a covalent enzyme-substrate intermediate, which is subsequently cleaved by an activated water molecule. The catalytic nucleophile Ser-149 mounts a nucleophilic attack at the sp^2 carbonyl carbon on activation by His260 (Fig. 2*C*). Simultaneously, His260 abstracts a proton from Ser-149. The negatively charged enzyme-substrate tetrahedral

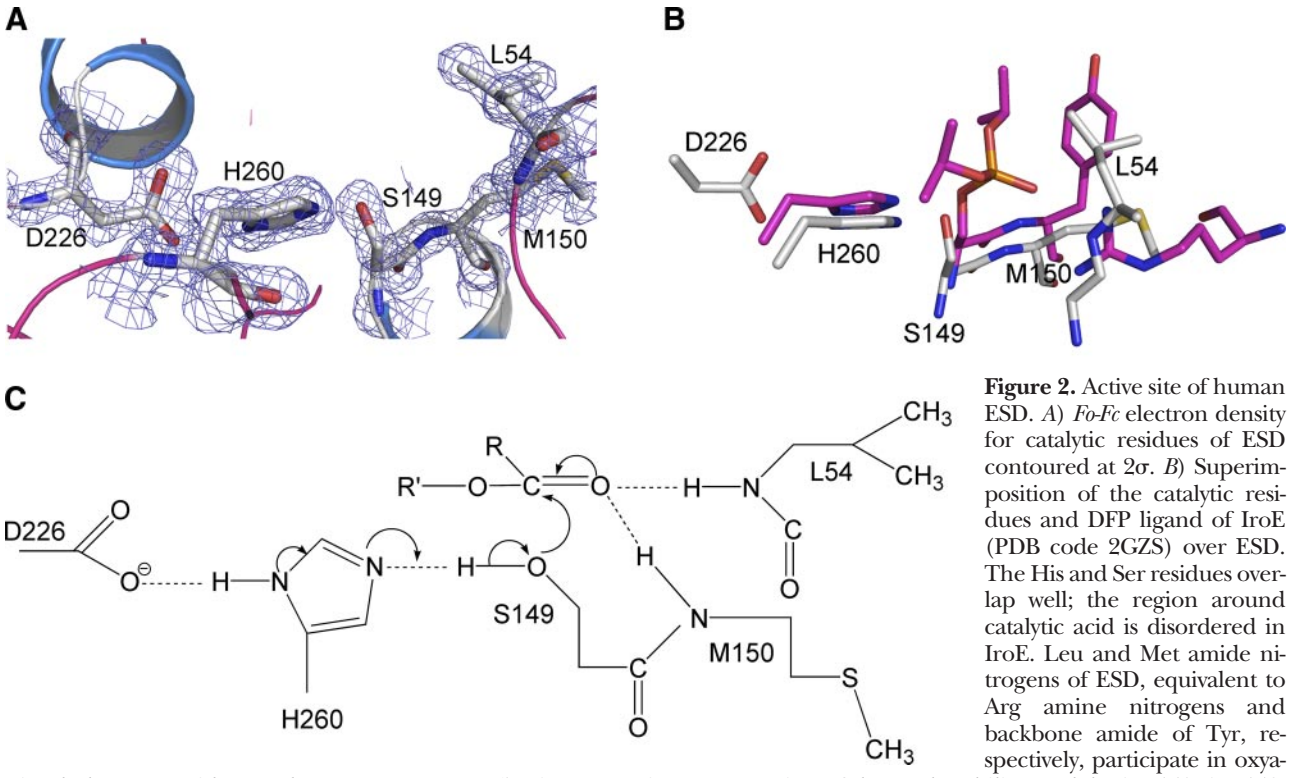

Figure 2. Active site of human ESD. *A*) *Fo-Fc* electron density for catalytic residues of ESD contoured at 2σ. *B*) Superimposition of the catalytic residues and DFP ligand of IroE (PDB code 2GZS) over ESD. The His and Ser residues overlap well; the region around catalytic acid is disordered in IroE. Leu and Met amide nitrogens of ESD, equivalent to Arg amine nitrogens and backbone amide of Tyr, respectively, participate in oxyanion hole. IroE residues and DFP are magenta. *C*) Diagrammatic representation of the nucleophilic attack by Ser-149. Ser-149, activated by His260, mounts a nucleophilic attack on the carbonyl carbon of the substrate. The intermediate is stabilized in an oxyanion hole formed by the backbone nitrogens of Met150 and Leu54.

intermediate thus formed is stabilized in the oxyanion hole by the main chain amide nitrogens of Met150 and Leu54, while the positively charged histidine is stabilized by interactions with the carboxyl oxygens of Asp226 (Fig. 2*C*). After the release of the alcohol, the acid part of the substrate now bound to the serine is released by a nucleophilic attack mounted by a water molecule activated by the histidine. This completes the hydrolysis reaction and returns the enzyme back to its native state.

Site-directed mutagenesis

Using the structure of ESD with a superimposed inhibitor DFP molecule as a guide, a number of amino acids were mutated in order to probe their role in the function of the enzyme (Table 2). The catalytic triad residues, Ser-149, Asp226, and His260, and the oxyanion hole related residues, Met150 and Leu54, were mutated to alanine. All the mutants were purified to homogeneity and tested for enzyme activity under identical conditions. Mutation of any of the catalytic triad residues to alanine almost completely abolished the enzymatic activity (Table 2). Thus, the catalytic triad residues of ESD are critical for activity. Interestingly, mutation of Met150 to alanine resulted in a 62% increase in enzyme activity, while a L54A mutation resulted in a 17% reduction in enzyme activity when compared to wild-type ESD (Table 2). Replacement of Met150 with alanine probably facilitates access to the active site by reducing steric hindrances imposed by the side chain of methionine. The decrease in activity of L54A mutation could be attributed to the possible loss of interaction of the methyl groups of Leu54 with the substrate. Leu54 probably plays a role in the docking of the substrate.

TABLE 2. *Relative activity of ESD mutants*

Mutation	Relative activity (%)
Wild type	100
S149A	NA
S149T	1.3
D226A	4.3
D226N	9
H260A	3
H260Q	1.3
L54A	83
M150A	162

NA, no activity.

DISCUSSION

Primary sequence alignment of homologs of ESD from different species revealed a number of highly conserved residues (**Fig. 3**). The catalytic triad residues and the oxyanion hole-related residues are absolutely conserved across species. We mapped the conserved residues on the structure of ESD (Fig. 3*B*). Interestingly, residues in and around the active site are absolutely conserved, indicating a common mechanism of catalysis. A search for structural homologs of ESD using the secondary structure matching server (www.ebi.ac.uk/msd-srv/ssm/cgi-bin/ssmserver) indi-

cated that the best match in terms of primary sequence identity and secondary structure was a yeast *S*-formylglutathione hydrolase (ySFGH) (26). ESD showed a 39.9% sequence identity and a *Z* score of 12.5 for 264 matching Cα atoms with a root mean square (RMS) deviation of 1.1 Å with this protein. Although the protein was deposited as a hypothetical protein in PDB, it was eventually shown to have *S*-formylglutathione hydrolase activity (26). However, the exact physiological role of this protein in yeast is still unknown. The catalytic triad and the oxyanion hole-related residues of ySFGH are similar to that of human ESD, indicating a conserved mechanism of catalysis (26).

The secondary structural elements of a virulence factor protein, esterase A, from *Streptococcus pneumoniae* (*Z* value 9.8, 214 overlapping Cα atoms with an RMS deviation of 1.8 Å) (27) and an antigen 85C from *Mycobacterium tuberculosis* (*Z* value 7.7, 226 overlapping Cα atoms with an RMS deviation of 1.9 Å) (28) also matched well with the structure of human ESD. A notable difference is the absence of strand β1 in the structure of esterase A and antigen 85C. In addition, the loop region connecting

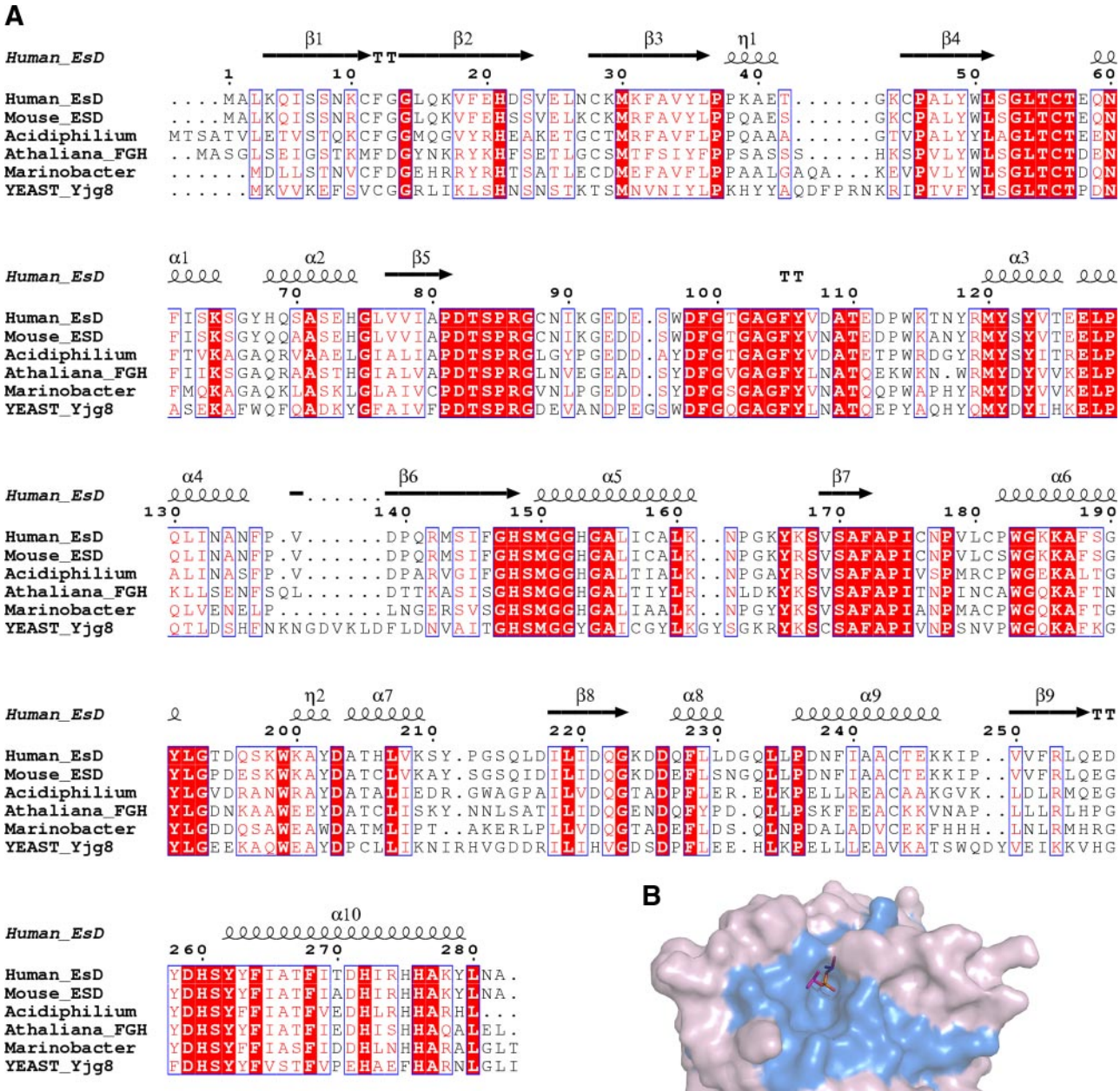

Figure 3. Conserved residues of human ESD. *A*) Primary sequence alignment of homologs of ESD. Absolutely conserved residues are highlighted in red. Secondary structural elements of human ESD are labeled. *B*) Mapping of absolutely conserved residues on the structure of ESD. Blue represents absolutely conserved residues. DFP ligand is shown as sticks.

strand β5 with helix α2 is much longer in ESD when compared to esterase A. In case of antigen 85C, this region is seen forming two short antiparallel strands. His148 sitting adjacent to the nucleophilic serine is replaced by a leucine in esterase A and antigen 85C, while Trp236 (Trp264 in antigen 85C) in the active site cleft of esterase A is substituted by Ile265 in ESD. Such minor differences in the active site define substrate specificities for individual esterases.

The structure of ESD determined in this study reveals a typical α/β-hydrolase fold with the characteristic catalytic triad residues. Interestingly, a wide variety of esterases with diverse substrate specificities perform catalysis using these conserved features. A number of insertions in the canonical α/β-hydrolase fold, close to the active site of ESD are observed. The insertions probably regulate access of the substrate to the active site and impart substrate specificities. Although the recombinant human ESD in our study did show activity against 4-methylumbelliferone acetate, the physiological substrate of the enzyme in the human body may be different. The key remaining question is the elucidation of the exact physiological role of this protein in the human body, which would also answer the question of whether it plays a role in the pathogenesis of RB. FJ

This work was funded by the National Natural Science Foundation of China (grants 20572063, 30670427, and 30721003), the Ministry of Science and Technology of China (grants 2006AA02A316 and 2006CB910901), the Ministry of Health of China (grant 2008ZX10404), the China Postdoctoral Science Foundation (20070420533), and a Chinese Academy of Sciences research grant (07CF09). Crystallographic data were collected at SER-CAT 22-ID beamline at the Advanced Photon Source (Argonne National Laboratory, Lemont, IL, USA). The use of the Advanced Photon Source was supported by the U.S. Department of Energy, Office of Science, Office of Basic Energy Sciences, under contract W-31-109-Eng-38. Atomic coordinates and structure factors of human esterase D have been deposited in the Protein Data Bank under accession code 3FCX.

REFERENCES

1. Sparkes, R. S., Sparkes, M. C., Wilson, M. G., Towner, J. W., Benedict, W., Murphree, A. L., and Yunis, J. J. (1980) Regional assignment of genes for human esterase D and retinoblastoma to chromosome band 13q14. *Science* **208,** 1042–1044
2. Young, L. J., Lee, E. Y. H. P., To, H., Bookstein, R., Shew, J. Y., Donoso, L. A., Sery, T., Giblin, M., Shields, J. A., and Lee, W. H. (1988) Human esterase D gene: complete cDNA sequence, genomic structure, and application in the genetic diagnosis of human retinoblastoma. *Hum. Genet.* **79,** 137–141
3. Schefler, A. C., Abramson, D. H. (2008) Retinoblastoma: what is new in 2007–2008. *Curr. Opin. Ophthalmol.* **19,** 526–534
4. Shields, C. L. Uysal, Y., Benevides, R., Eagle, R. C., Jr., Malloy, B., and Shields, J. A. (2006) Retinoblastoma in an eye with features of Coats' disease. *J. Pediatr. Ophthalmol. Strabismus* **43,** 313–315
5. Sparkes, R. S., Murphree. A. L., Lingua, R. W., Sparkes, M. C., Field, L. L., Funderburk, S. J., and Benedict, W. F. (1983) Gene for hereditary retinoblastoma assigned to human chromosome 13 by linkage to esterase D. *Science* **219,** 971–973
6. Frydman, M., Bonne-Tamir, B., Farrer, L. A., Conneally, P. M., Magazanik, A., Ashbel, S., and Goldwitch, Z. (1985) Assignment of the gene for Wilson disease to chromosome 13: linkage to the esterase D locus. *Proc. Natl. Acad. Sci.* **82,** 1819–1821
7. Cowell, J. K., Thompson, E., and Rutland, P. (1987) The need to screen all retinoblastoma patients for esterase D activity: detection of submicroscopic chromosome deletions. *Arch. Dis. Child.* **62,** 8–11
8. Lee, E. Y., and Lee, W. H. (1986) Molecular cloning of the human esterase D gene, a genetic marker of retinoblastoma. *Proc. Natl. Acad. Sci.* **83,** 6337–6341
9. Squire, J., Dryja, T. P., Dunn, J., Goddard, A., Hofmann, T., Musarella, M., Willard, H. F., Becker, A. J., Gallie, B. L., and Phillips, R. A. (1986) Cloning of the esterase D gene: a polymorphic gene probe closely linked to the retinoblastoma locus on chromosome 13. *Proc. Natl. Acad. Sci.* **83,** 6573–6577
10. Lee, W. H., Brookstein, R., Hong, F., Young, L. J., Shew, J. Y., and Lee, E. Y. (1987) Human retinoblastoma susceptibility gene: cloning, identification, and sequence. *Science* **13,** 1394–1399
11. Yuzbasiyan-Gurkan, V., Wagnitz, S., Blanton, S. H., and Brewer, G. J. (1993) Linkage studies of the esterase D and retinoblastoma genes to canine copper toxicosis: a model for Wilson disease. *Genomics* **15,** 86–90
12. Okunuki, Y., Usui, Y., Kezuka, T., Hattori, T., Masuko, K., Nakamura, H., Yudoh, K., Goto, H., Usui, M., Nishioka, K., Kato, T., and Takeuchi, M. (2008) Proteomic surveillance of retinal autoantigens in endogenous uveitis: implication of esterase D and brain-type creatine kinase as novel autoantigens. *Mol. Vis.* **14,** 1094–1104
13. Loughna, S., Bennett, P., Gau, G., Nicolaides, K., Blunt, S., and Moore, G. (1993) Overexpression of esterase D in kidney from trisomy 13 fetuses. *Am. J. Hum. Genet.* **53,** 810–816
14. Varki, A., Muchmore, E., and Diaz, S. (1986) A sialic acid-specific O-acetylesterase in human erythrocytes: possible identity with esterase D, the genetic marker of retinoblastomas and Wilson disease. *Proc. Natl. Acad. Sci. U. S. A.* **83,** 882–886
15. Harms, N., Ras, J., Reijnders, W. N., van Spanning, R. J., and Stouthamer, A. H. (1996) S-Formylglutathione hydrolase of *Paracoccus denitrificans* is homologous to human esterase D: a universal pathway for formaldehyde detoxification? *J. Bacteriol.* **178,** 6296–6299
16. Lee, W. H., Wheatley, W., Benedict, W. F., Huang, C. M., and Lee, E. Y. (1986) Purification, biochemical characterization, and biological function of human esterase D. *Proc. Natl. Acad. Sci. U. S. A.* **83,** 6790–6794
17. Eiberg, H., and Mohr, J. (1986) Identity of the polymorphisms for esterase D and S-formylglutathione hydrolase in red blood cells. *Hum. Genet.* **74,** 174–175
18. Stols, L., Gu, M., Dieckman, L., Raffen, R., Collart, F. R., and Donnelly, M. I. (2002) A new vector for high-throughput, ligation-independent cloning encoding a tobacco etch virus protease cleavage site. *Protein Exper. Purif.* **25,** 8–15
19. Otwinowski, Z., and Minor, W. (1997) Processing of X-ray diffraction data collected in oscillation mode. *Methods Enzymol.* **276,** 307–326
20. Lebedev, A. A., Vagin, A. A., and Murshudov, G. N. (2008) Model preparation in MOLREP and examples of model improvement using X-ray data. *Acta Crystallogr. D Biol. Crystallogr.* **64,** 33–39
21. Murshudov, G. N., Vagin, A. A., and Dodson, E. J. (1997) Refinement of macromolecular structures by the maximum-likelihood method. *Acta Crystallogr. D Biol. Crystallogr.* **53,** 240–255
22. Brünger, A.T. (1992) Free R value: a novel statistical quantity for assessing the accuracy of crystal structures. *Nature* **355,** 472–475
23. Emsley, P., and Cowtan, K (2004) Coot: model-building tools for molecular graphics. *Acta Crystallogr. D.* **60,** 2126–2132
24. Davis, I. W., Murray, L. W., Richardson, J. S., and Richardson, D. C. (2004) MOLPROBITY: structure validation and all-atom contact analysis for nucleic acids and their complexes. *Nucleic Acids Res.* **32,** 615–619
25. Larsen, N. A., Lin, H., Wei, R., Fischbach, M. A., and Walsh, C. T. (2006) Structural characterization of enterobactin hydrolase IroE. *Biochemistry* **45,** 10184–10190
26. Legler, P. M., Kumaran, D., Swaminathan, S., Studier, F. W., and Millard, C. B. (2008) Structural characterization and reversal of the natural organophosphate resistance of a D-type esterase, *Saccharomyces cerevisiae* S-formylglutathione hydrolase. *Biochemistry* **47,** 9592–9601
27. Kim, M. H., Kang, B. S., Kim, S., Kim, K. J., Lee, C. H., Oh, B. C., Park, S. C., and Oh, T. K. (2008) The crystal structure of the estA protein, a virulence factor from *Streptococcus pneumoniae*. *Proteins* **70,** 578–583
28. Ronning, D. R., Klabunde, T., Besra, G. S., Vissa, V. D., Belisle, J. T., and Sacchettini, J. C. (2000) Crystal structure of the secreted form of antigen 85C reveals potential targets for mycobacterial drugs and vaccines. *Nat. Struct. Biol.* **7,** 141–146

Received for publication November 4, 2008.
Accepted for publication December 4, 2008.